# 5

# Temperature profile of the receiver Detection at far-field using infrared detectors

Ray tracing methods, as mentioned in the previous chapter, enable us to estimate the stagnation temperature profile of the receiver in a given solar field. Further, the optical efficiency of the heliostat field as mentioned, may also be estimated. In order to safeguard the receiver from reaching high temperature for a given incident flux, which could lead to permanent damage on it, it is beneficial to perform an investigate on the temperature contours on the receiver in central receiver systems. This method could assist in estimation of contribution radiative losses on the receiver, if any.

The investigation on the temperature profile of the receiver using concentration and stagnation temperature were performed as discussed in chapter 2 and chapter 3.

The central receiver considered in these investigations were usually kept at the top of the tower to perform beam-up configuration design. The spatial profile of the temperature depends on various factors like irradiance, number of heliostats, aberration contribution from the heliostats and non-uniformity of the receiver due to its manufacturing effects among others. As the radiation reflected from the heliostat is incident onto the receiver, the temperature of the receiver increases from the ambient during the operational hours. As discussed above, various factors contributing to the non-uniform high temperature region on the receiver, are often referred as hot-spots. These hot-spots permanently damages the receiver in a given region, if the incident flux is above the damage threshold of the materials (for most of the materials it is between 100 $kW/m^2$ to 500 $kW/m^2$). Since, the temperature of the receiver is finite and above the ambient temperature, the radiation emitted would be Planckian in nature [147,153]. By observing emission from the receiver in the various spectral regions, i.e., near infrared and other bandwidths within the infrared region at a far-field from the receiver, as a non-contact method during the operational hours would be advantageous for its specified functioning and also, monitoring/avoiding hot-spots formation on it.

Considering spatial profiles of the concentration and stagnation temperature on the receiver, the amount radiation emitted by the receiver were estimated. For the calculation purposes, emissivity = 0.1 was considered for the receiver, since a protective coating is provided to it, so as to reduce the radiative losses from it [67, 147, 153-157] in a given bandwidth per unit area ($m^2$). The estimation of the concentration on the receiver based on flux map was recorded using Tracepro® and a representation of it is shown in fig 5.1 below.

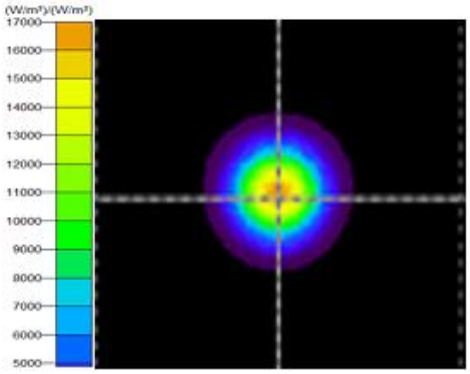


Fig 5.1 A flux profile at the receiver at 1200 hour (December 27th) using Tracepro.

The image of flux map along with its distribution on the receiver was recorded using Tracepro from 900 hrs-1600 hrs on December 27th [83]. Flux at each individual location (coordinates be x,y) provides the amount of concentration on the receiver in a specified position. Since the temperature (concentration) profile is non-uniform over the receiver, the stagnation temperature distribution was estimated using digitized data of (flux-profile) image on the receiver having elements of 128 x 128 considered for statistical distribution. A typical example of stagnation temperature distribution is shown in the fig 5.2 below. Using the solar irradiance at Jodhpur at a specified time and concentration at a given position on the receiver, the stagnation temperature associated with it was estimated [146-155].

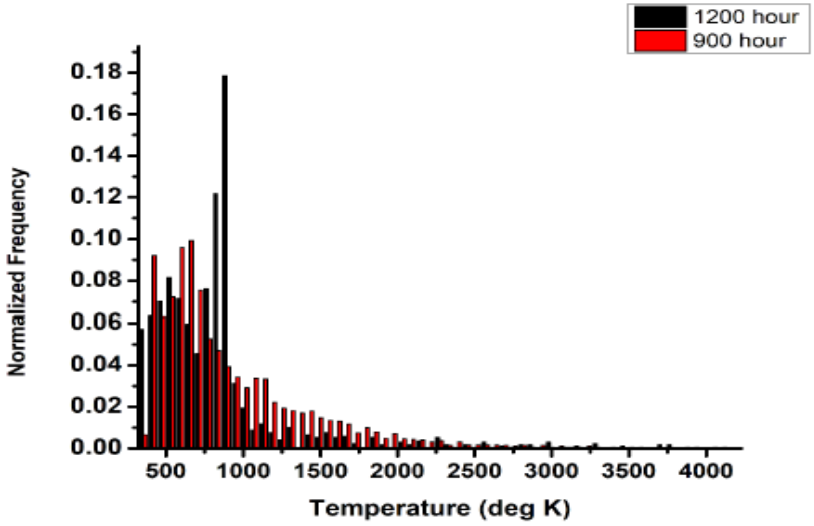


Fig 5.2 : Stagnation Temperature distribution at the receiver 900 hour and 1200 hour [155]

To estimate the amount of radiative emission (in the unit of W) in various bandwidth at the receiver from the estimated stagnation temperature and radiation at far field using appropriate calculations [147-155] using Planck radiation law. The radiative emission in the infrared region coming from the receiver due to its high temperature (stagnation) during the operational hours may be detected at the ground using appropriate infrared detector and emitted radiation would

follow Planckian nature as discussed above. As the rays are focused onto the receiver from the heliostats, the contours of concentration profiles obtained on the receiver. A proposed far field infrared measurement scheme due to Planckian emission of the receiver is shown in figure 5.3.
This estimation of temperature distribution was employed using infrared estimation tool namely PYRADI® [154], based on Planckian law, the amount of radiation ( in the unit of W) was estimated in various bandwidth region at the receiver as well as far field using appropriate calculations [147, 153-157]. The radiative emission coming from the receiver due to its high temperature during the operational hours may be detected at the ground using appropriate infrared detector and emitted radiation would follow Planckian nature. As the temperature of the receiver varies between 300 K (ambient temperature) and stagnation temperature 3000 K, the Planckian emission would be peaked in the infrared region [67,147, 153-160].
Detection of an infrared signal using a suitable detector kept on the ground enables to predict the temperature profile as well as emissivity of the receiver. For this investigation, the infrared radiations from the receiver are collected over an area 16 $cm^2$ kept on the ground using appropriate optics and its falls onto a IR-detector having active area of 0.01 $cm^2$ , since dimensions of the available IR-detectors are small [156]. For collection of IR-radiations, collection optics with large area may be chosen so as to have a better signal to noise ratio (SNR) and the collection optics at kept at a distance of 28 meter from the receiver as shown in Figure 5.3. The chief objective of this investigation is to study temperature profile of receivers under a realistic scenario using few commercially available IR-detectors and the measurements associated with it. Thus, the choice of compatible IR-detectors can be arrived with a help of ray tracing technique and the infra-red prediction tool PYRADI®.

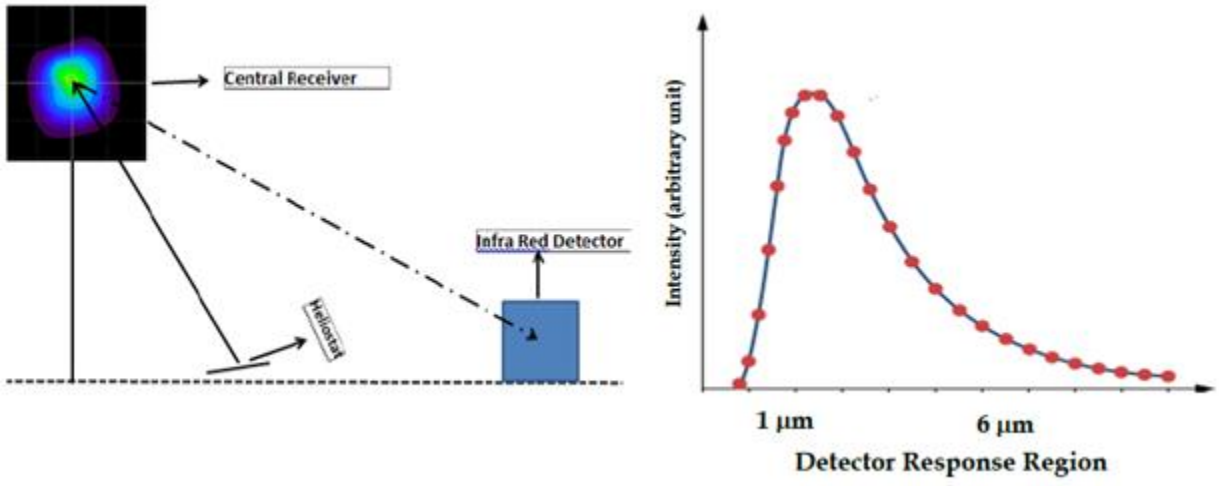


Fig 5.3 A simplified schematic representation to calculate Planckian emission of the receiver at far field using infrared detector

The stagnation temperature of the receiver was estimated using equation was discussed in *Chapter 2*. In order to investigate radiation emitted by the receiver and the required measurements

for a realistic scenario,two semiconductor based detectors were used, namely InGaAs and InSb, having wavelength response regions 1- 2.05 μm and 1 - 6 μm respectively were chosen for this purpose. In the following section, is a brief discussion on the details of detectors responsivity, noise equivalent power (NEP) and detectivity were presented. Stoddard and Bergan [161] has carried out extensive evaluation of infrared thermographs to solar central receiver temperature measurements using appropriate telescopic arrangement for the monitoring it. Recently, Rakhman and Blokland [162] has carried out non-contact surface temperature measurements of nanocrystalline diamond foil under intense ion beams using similar telescopic arrangements for the measurement of temperature. Our work completely consistent with the work carried out by Bergan. The proposed twin-wavelength photodetector is a novel as well as inexpensive to monitor the central receiver from a far-field for its health monitoring.

### Responsivity

The term responsivity [156] is used to describe the amplitude of electric signal with respect to the incident flux. Responsivity is a function of wavelength or temporal frequency.

$$R(\lambda, f) = \frac{I_{out}}{\Phi_{incident}} = \frac{I_{out}}{E(\lambda,f)A_d} \qquad [\mathrm{A/W}]5.1$$

where$I_{out}$ is the detector output current, $\Phi_{incident}$is incident flux in Watts, E $(\lambda, f)$ is incident irradiance in watts per square centimeter and $A_d$ is the detector area in centimetre square.

### Noise Equivalent Power

The noise equivalent power (NEP) is a measure of the ultimate sensitivity of a given detector and it is a convenient number to use to estimate what the signal to noise ratio (S/N) will be if the power available is known [156]. NEP is the power that must fall on the detector to cause an S/N of 1.

$$NEP = \frac{Noise}{Responsivity}\ [\mathrm{Watt}]$$

A variant uses the noise spectral density instead of the noise in the NEP formula. It is the NEP per unit band width (NEP').

$$NEP' = \frac{Noisespectraldensity}{Responsivity}$$

$$NEP' = \frac{Noise}{\sqrt{(\Delta f)}Responsivity} \qquad [\mathrm{W/Hz^{1/2}}]$$

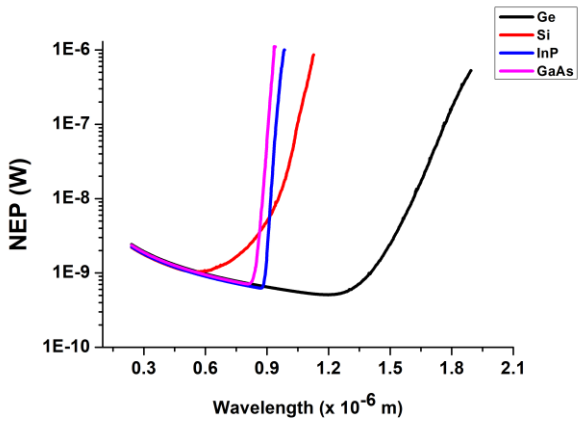


Figure 5.4 : Spectral Noise Equivalent Power of Si, Ge, GaAs, InP

### *Spectral* Detectivity

The Noise equivalent power (NEP) is convenient for predicting the minimum power required for a given detector can detect as a noise and higher than that would appear as signal. A good detector will have a small NEP. Detectors of different sizes will have different NEPs. In light of this, NEP cannot be good measure for the selection of the detector, unless we specify the size of the detector.

The specific Detectivity D*, now normally just called Detectivity or D star ($D^*$). $D^*$ eliminates those two drawbacks. A large value for D* is good choice for the selection of a detector. The D* is defined as

$$D^* = \frac{responsivity * \sqrt{Area}}{noise\ spectral\ density}$$

$$D^* = \frac{R * \sqrt{A_d}}{N/\sqrt{\Delta f}}$$

$$D^* = \frac{\sqrt{Area} * \sqrt{\Delta f}}{NEP} \vee D \quad = \frac{signal * \sqrt{\Delta f}}{noise * incidence * \sqrt{Area}}$$

where S is signal in unit [W], N is noise in unit [W], incident flux E in Watt and $A_d$ is the area of detector. The unit of D* are cm $(Hz)^{1/2}/W$.
D* is useful in predicting signal to noise ratio (S/N) in a given test environment.

$$\frac{S}{N} = D \quad \frac{incidence * \sqrt{A_d}}{\sqrt{\Delta f}} \qquad 5.2$$

Noise Equivalent Power for the semiconductors namely: Silicon (Si), Germanium (Ge), Gallium Arsenide (GaAs) and Indium Phosphate (InP) are shown in Figure 5.4. We restrict out investigations with two semiconductors for infrared detectors namely InGaAs and InSb for our investigation. A theoretical estimation for D* [157-160,163-169] for InGaAs and InSb for a wavelength region from 1-6 $\mu m$ were computed using equation 5.2 and shown in fig 5.5 next page at the frequency $\Delta f = 1500\ Hz$ , area of the detector $A_d$ = 1 mm². Using the real ($n$) and imaginary ($k$) component of refractive indices from the available data for InGaAs and InSb [168,169] absorption coefficient and quantum efficiency were estimated (not shown here).

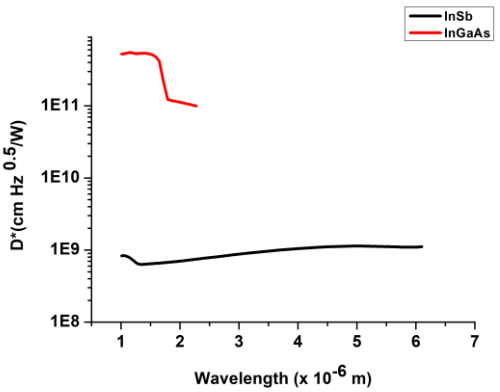


Figure 5.5: The specific detectivity D* for InGaAs and InSb in the infrared wavelength region.

The considered dark current were$2 \times 10^{-9} 3 \times 10^{-12} Amp$ for InSb and InGaAs respectively. The behavioral pattern is similar to the commercially available infrared detectors (Fig 5.6 below)

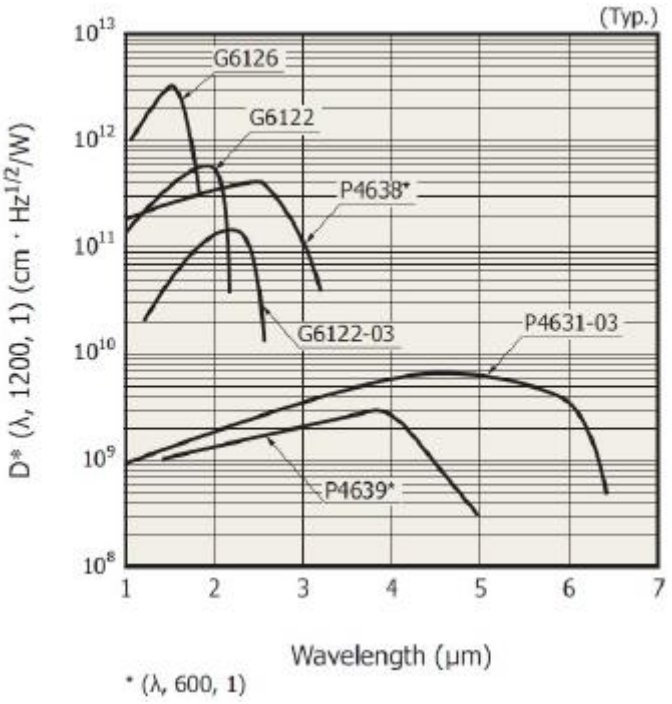

Fig 5.6: **T**he specific detectivity profile take from Hamamatsu technical report [170] for two infrared detectors namely InSb (curve: P4631-03) and InGaAs (curve: G6122)

## Estimation of radiation measurement at far field from the receiver

To estimate the radiation incident on the infrared detector, temperature profile of the receiver at 1200 hours (Day: 27th December) was considered. Using Tracepro®,the concentration on individual spatial position was computed on the receiver with flux-map and its corresponding stagnation temperature using the solar irradiance data [171] . A typical stagnation temperature profile of the receiver is shown in Fig 5.7. Each individual area (digitized) of the receiver was 0.0015259 $m^2$ and provided varying temperature zones along with corresponding areas from the receiver. The estimated amount of total (infrared region bandwidth namely1- 2.05 µm and 1 - 6 µm) power on the collection optics kept at the ground (area: 4 cm x 4 cm) are carefully computed.

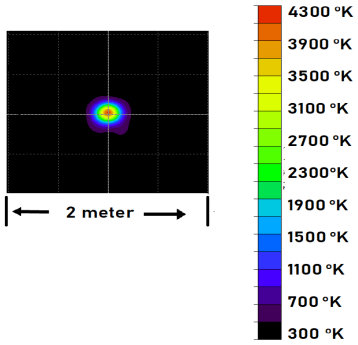


Fig 5.7: A stagnation temperature profile of the receiver on December 27th at midday (1200 hours)

To estimate the total power reaching the infrared detector at two different bandwidth regions, we have used normalized frequency (w. r. t. total number of pixels) for the temperature distribution on the receiver. For example, at 1200 (Day: December 27th) to estimate the total power on the infrared detector (at the ground) using infrared prediction tool, the estimated values were 3.81 MW and 5.93 mW for the wavelength regions 1- 2.05$\mu m$ and 1-6 $\mu m$respectively. Using the available D* data from the original manufacturer's of the infrared detectors, we estimate the correspond D* and NEP for the employed infrared detectors in the specified spectral bandwidth and it is listed in Table 5.1.

| Sl. | Wavelength Region | $D^*$ (#) (cm Hz 0.5 /W) | NEP (W) |
|---|---|---|---|
| 1 | 1 - 6 µm | $9 \times 10^{9}$ | $3.85 \times 10^{-10}$ |
| 2 | 1 - 2.05 µm | $5.15 \times 10^{11}$ | $5.96 \times 10^{-12}$ |

Table 5.1 : Two range of D* and NEP analysis

These values(#) are obtained for the entire range of wavelength as specified in column 2 above table 5.1. The integrated infrared radiation in the two different regions were much higher than that of NEP. Thus, one can prove unambiguously that the choice of the detector employed would be helpful in monitoring the receiver.

Using the above approach, we defined the average temperature on the receiver as

$$T_{avg} = \frac{\sum_i T_I n_i}{\sum_i n_i}$$

where $T_i$ is the temperature at the $i^{th}$ position (*label*) on the receiver and $n_i$ number of times $T_i$ appearing on the receiver. Using the above relation, estimation for average temperature ($T_{avg}$ was found to be 880 K for beam-up configuration at 1200 hours (Day: December 27th ), while we estimated temperature for CPC with beam-down approach as 1090 K during the same operational hours. The increase in the temperature is clearly an indicative of the presence of CPC in the system.

| Date | Time(hrs) | Solar Irradiance ($w/m^2$) | Total Power (Mw) (λ range 1-2.05 μm) | Total Power (Mw) (λ range 1-6 μm) | Ratio of power (Mw) (λ range 1-6 μm) |
|---|---|---|---|---|---|
| | 900 | 550 | 3.03 | 7.02 | 0.42 |
| | 1000 | 980 | 3.7 | 6.36 | 0.58 |
| | 1200 | 980 | 3.81 | 5.92 | 0.64 |
| | 1400 | 710 | 2.51 | 4.24 | 0.59 |
| 2712 | 1600 | 300 | 0.98 | 1.69 | 0.57 |

Table 5.2: Integrated power at two different infrared bandwidth regions at far-field using stagnation temperature of the receiver.

The Planckian emission in infrared region arising out of the central receiver in a given heliostat field due to its temperature profile and its distribution were analyzed at a far field from the receiver and shown in above table 5.2. The ratio of the integrated power in lower bandwidth region to higher bandwidth region is highest at the midday could be attributed to higher temperature as the Planckian curve shifts towards lower wavelengths. The highest total power observed at 900 hours (27th December) could be a combination of aberration of Sun image (Sun is further away from zenith at 900 hour) formation at the receiver and lower temperature as compared to midday. Further, it can be concluded that, a few commercially available infrared detectors can be employed to measure the integrated power at two different bandwidth regions. The estimated value using ray tracing technique as well as infrared prediction tool

unambiguously confirms that the integrated power at two different bandwidth regions as much higher than that of NEP of the detector, which would enable the researchers to choose appropriate detectors based on the receiver and heliostat field conditions.

This is to summarize that in this investigation on the temperature distribution profile of the receiver for a heliostat field were done using flux profile obtained from ray tracing technique and their corresponding average temperatures and stagnation temperatures were estimated. Increase in average temperature on the receiver was noted by introducing CPC as a secondary concentrator. The specific detectivity (D*) for two different infrared detects were estimated along with their NEP's. The total integrated power over a responsivity (i.e. Quantum Efficiency curve) in a considered bandwidth for the two different detectors were six order magnitude higher than that of the NEP of the detectors. This approach can widely be used for performance monitoring of the central receiver systems in various concentrated solar fields.

## 5.1 Estimation of receiver temperature

To validate the use optical detectors regarding estimation of receiver temperature, a simple experiments were carried out using a commercially available photo-detectors with their known responsivity curve. For this purpose, we have used Silicon Photodiode with amplifier (Thorlabs, USA, Model: PDA10A2), has an active area of 0.8 $mm^2$. The initial calibration were done using a CW laser ( HeNe Laser, wavelength = 632.8 nm, optical power: 2 milli-Watt (mW)) and the outputs were measured using an Oscilloscope and a multimeter. The incident input power of the laser was varied between micro-Watt (µW) to milli-Watt (mW) using optical attenuators and also, the entire optical beam was made to fall on the active area of the detector. The incident input power of the laser was kept at 2 mW, 200 µW and 2 µW, while 2.24, 0.220 and 0.0022 Volts were observed as output voltage of the photodiode. To record the broad band emission from a receiver, experiments were carried out to recorded the output voltage of the solar radiation at three different band-widths using appropriate interference filter before the photo-diode. The solar spectrum was recorded using a broad band spectrometer (Ocean Optics, Model: Red-hat) and the observed full-width half-maxima (FWHM) spectrum found to be 225 nm. Using interference filters at 800 ± 40 *nm*, 810 ± 10 *nm* and 694 ± 10 nm the estimated optical power 868 W $m^{-2}$, 693 W $m^{-2}$ and 912 W $m^{-2}$. The recorded optical using hand-held solar power meter was found to be 760 W $m^{-2}$ during the experimental observation.

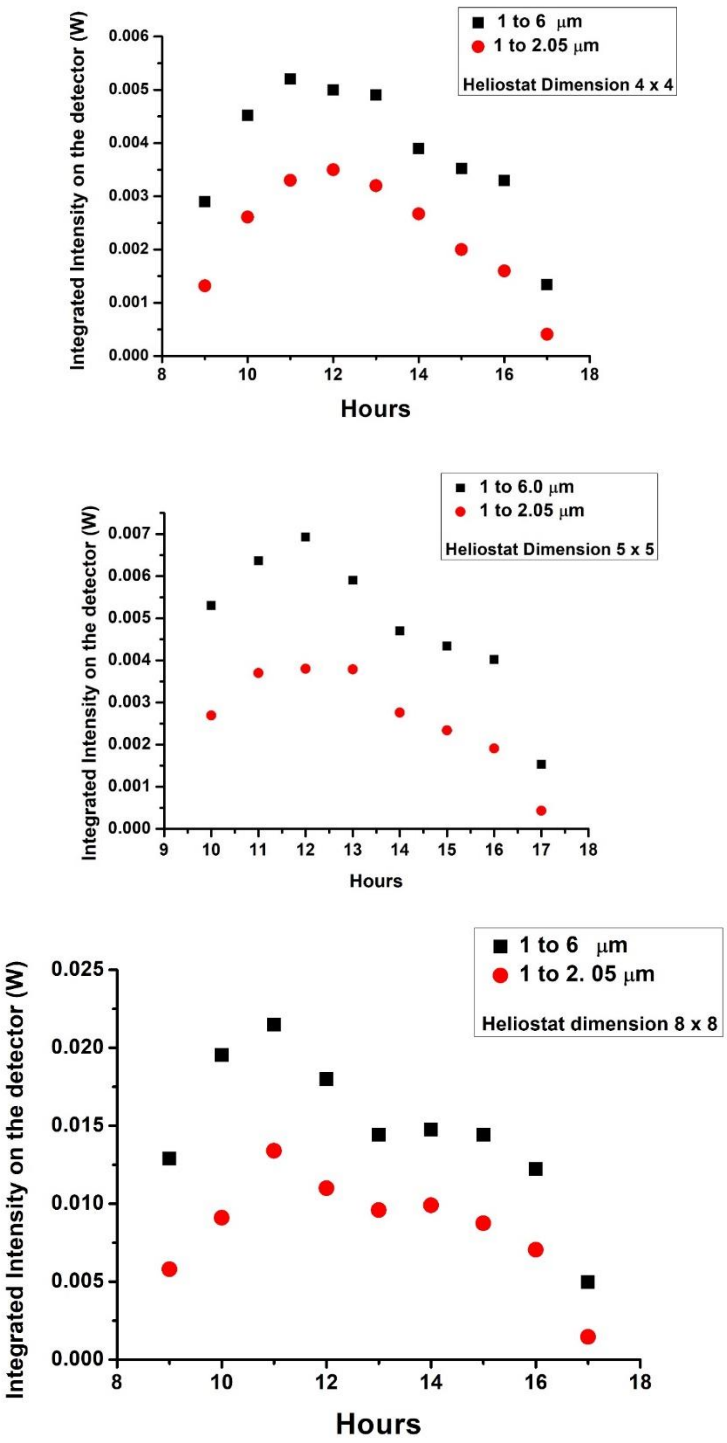


***FIGURE 5.8*** : Integrated intensity of Planckian emission in two different band-widths of infrared region regions ((two detectors InSb (1 μm to 6 μm) and InGaAs (1 μm to 2.05 μm)) for heliostat dimensions: (a) 4 meter x 4 meter, (b) 5 meter x 5 meter and (c) 8 meter x 8 meter.